Localization and resonant transmission of third-sound waves on a random substrate

C. A. Condat
Institute for Physical Science and Technology, University of Maryland, College Park, Maryland 20742

T. R. Kirkpatrick
Department of Physics and Astronomy and Institute for Physical Science and Technology, University of Maryland, College Park, Maryland 20742

(Received 11 October 1985)

The analysis of a recently proposed experiment, designed to study the one-dimensional localization of third-sound excitations, is extended to higher frequencies. Transmission resonances are predicted for a discrete set of frequencies. The disorder is introduced by randomly distributing identical parallel strips of a modified substrate. These strips can be produced in such a way that they either modify the thickness of the part of the superfluid film located on the strips or change the effective third-sound speed in these regions. The main features of the localization and the transmission resonances are studied in detail. The system described here is shown to be conceptually far simpler than its electronic analogs. Experimentally, the analogs of inelastic scattering and interaction effects in the electron problem can be easily controlled.

I. INTRODUCTION

Since the early work of Mott and Twose[1] and Borland,[2] the problem of electron localization in one dimension has been the subject of a considerable amount of research. In the references we list several review articles.[3-5] A number of rigorous results have also been obtained.[3,6-8]

It has been shown that all electronic states (except for a set of measure zero) in random one-dimensional systems are localized. In usual experimental situations at low temperatures the conductivity is determined by thermally activated hopping.[9,10] However, Lifshitz and Kirpichenkov have investigated the tunneling of quantum particles through a disordered array of δ-function barriers[11] and found that a particle with an energy near that of an eigenvalue of the random Hamiltonian would find the disordered region almost transparent. Azbel has studied the problem of localization by a random distribution of scatterers located on a finite one-dimensional lattice. He showed that such a system has transmission resonances.[12,13] Azbel has also considered finite-temperature effects in his model.[14] He showed that the conductance $G(T)$ should have the same type of temperature dependence as thermally activated hopping, i.e., $\ln G(T) \sim -T^{-1/2}$. Under certain circumstances a different temperature dependence has also been predicted.[15]

The conduction at very low temperatures can therefore proceed by two mechanisms: thermally activated hopping and resonance transmission. The first (second) is expected to be dominant when the inelastic characteristic length l_i is smaller (greater) than the sample length l.[15]

A further complication in the analysis of the transport processes at low temperatures is the presence of the electron-electron interaction.[16] In disordered systems this effect is more important than in ordered ones.

Currently, a significant theoretical and experimental effort is being devoted to the analysis of transport phenomena in one-dimensional electronic systems. The goal is the separation of the contributions to the conductivity.[17]

Less attention has been given to nonelectric localization problems.[18] This situation is beginning to change. Jäckle analyzed the conditions for experimental observation of phonon localization in nearly-one-dimensional solids;[19] McGurn *et al.* studied the contributions arising from the localization of surface polaritons to the scattering of polarized light by a randomly rough grating;[20] Baluni and Willemsen considered the transmission of acoustic waves through a sequence of alternating layers with random thicknesses.[21] Pendry and Kirkman investigated how disorder restricts the bandwidth available for signaling purposes in various one-dimensional systems.[22]

Recently, we proposed an experimental arrangement that should permit the detection of localized one-dimensional acoustic waves.[23] The excitations that are localized are third-sound wave and the randomness is introduced by a disordered array of parallel identical strips of a second substrate. We studied only the case of long-wavelength excitations (the Rayleigh scattering limit), for which the localization length ξ as a function of the frequency E decreases as $\xi \sim E^{-2}$.[13,21,24] Cohen and Machta suggested another experiment to localize third-sound waves;[25] they propose a two-dimensional system in which the disorder is introduced by dusting with small particles an otherwise clean substrate.

In this paper we extend the investigation initiated in Ref. 23 to higher frequencies and we also consider a second type of scatterers obtained by roughening random strips of the substrate. Localization and resonant transmission are predicted to occur under conditions which can be obtained experimentally with relative ease. Their analysis is simpler than in the electronic problem, since (A) at sufficiently low temperatures (below a few tenths of a degree Kelvin), the intrinsic attenuation length (for the uniform substrate) can be made extremely large

(indeed, much larger than any possible experimental substrate). The analog of the inelastic electron-phonon scattering effects can therefore be neglected. The condition $l_i \gg l$ for resonant tunneling is then satisfied. (B) The interaction between excitations (expressed through the nonlinear terms in the hydrodynamic equations) can be made arbitrarily small by controlling their amplitude. (C) The scatterers are macroscopic and can be built essentially identical to each other. As a consequence there is a closer correspondence between theory and experimental reality.

The details of the proposed system are explained in Sec. II. We use multiple-scattering techniques[26] to transform the boundary-value problem arising from the random distribution of scatterers into an equivalent many-body problem. We then calculate a configuration-averaged Green's function, obtaining a renormalized speed of sound and an attenuation length.

In Sec. III we use a diagrammatic formalism, previously applied by one of us to study the localization of sound waves by a random array of hard-sphere scatterers,[27] to calculate the intensity propagator. The intensity propagator is related to the configurational average of the squared Green's function, and it can be calculated by solving a kinetic equation. First, we solve it using a ladder approximation, which yields the Boltzmann diffusion coefficient. We then sum the maximally crossed diagrams and use the self-consistent approximation of Vollhardt and Wölfle[28] to obtain a transcendental equation for the localization length. This equation is solved and transmission resonances are predicted and analyzed.

Section IV contains a final discussion of the advantages and limitations of the system discussed here. Finally, in Appendix A we give the exact form of the T matrix, and in Appendix B we treat the effect of a nonvanishing intrinsic dissipation in the calculations of Sec. II.

II. THE PROPOSED SYSTEM AND THE AVERAGED GREEN'S FUNCTION

A. Background: A superfluid film on a stripped film on a stripped substrate

The theory of third-sound modes on a thin helium film is similar to the theory of shallow water waves, except that the restoring force is provided by the van der Waals interaction between the helium film and the atoms in the substrate.[29]

The properties of the third-sound excitations are substantially modified if we place on the original substrate an array of parallel identical strips of a second substrate. (See Fig. 1.) Since the equilibrium film thickness, which is determined by the van der Waals interaction, is modified when going from one substrate to the other,[30] the portion of the film located on a strip acts effectively as a scatterer for the third-sound waves. To a good approximation, the equilibrium thickness on a strip, h_2, is related to that on the original substrate, h_1, by the equation $h_2/h_1=(\alpha_2/\alpha_1)^{1/2}$, where α_2 and α_1 are the respective van der Waals force constants. The phase velocity of third sound, c, is the same on both regions. We will call

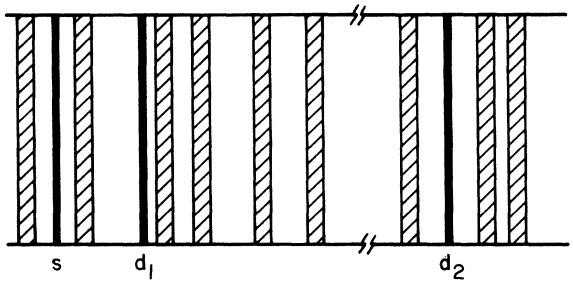

FIG. 1. Sketch of the random arrangement of parallel strips of a modified substrate. The positions of a detector d_1 close to the source s and of a second detector d_2 far from it are indicated.

these strips van der Waals (vDW) scatterers.

We assume that the temperature is low enough so that the normal helium component can be neglected. Given the relatively long wavelength of the third-sound waves we will also neglect surface tension.

The velocity potential $\phi(x)$, whose spatial derivative $v_s=\partial\phi/\partial x$ is the velocity of the superflow, satisfies the differential equation

$$\frac{\partial^2\phi}{\partial x^2}-\frac{1}{c^2}\frac{\partial^2\phi}{\partial t^2}-\frac{\Gamma}{c^2}\frac{\partial\phi}{\partial t}=0\ . \tag{2.1}$$

Here, Γ is a phenomenological damping constant,[31,32] which accounts for the residual ($T\to 0$) damping of third-sound excitations and which has been interpreted by Rutledge and Mochel as a surface friction.[31] Experiments performed using a uniform (no strips) vitreous quartz substrate yield $\Gamma h\approx 1.0$ atomic layers/sec.[31] Since this turns out to be a very small value when compared to the attenuation due to substrate disorder, we leave the discussion of the effects of intrinsic dissipation for Appendix B and set $\Gamma=0$ in the remainder of the text. (Note, however, that the lifetime of the localized excitations to be discussed in Sec. III will be determined by Γ. We estimate it to be of the order of seconds.)

The boundary conditions can be derived by noting that the region where the film thickness changes is very narrow for thin films.[30] If d is the distance over which the thickness changes, λ the third-sound wavelength, and a the strip half-width, we will have, in general, $d\ll\lambda$ and $d\ll a$. Consequently, the waves effectively react to a sudden variation in the film thickness at the edges of the strips. If X_j is the position of the center of the jth strip, the boundary conditions are

$$\begin{aligned}
&\phi_{j-1}(x,t)=\phi_j^s(x,t) \quad \text{at } x=X_j-a\ ,\\
&h_1\frac{\partial\phi_{j-1}}{\partial x}(x,t)=h_2\frac{\partial\phi_j^s}{\partial x}(x,t) \quad \text{at } x=X_j-a\ ,\\
&\phi_j^s(x,t)=\phi_j(x,t) \quad \text{at } x=X_j+a\ ,\\
&h_2\frac{\partial\phi_j^s}{\partial x}(x,t)=h_1\frac{\partial\phi_j}{\partial x}(x,t) \quad \text{at } x=X_j+a\ .
\end{aligned} \tag{2.2}$$

Here, ϕ_j^s is the velocity potential for the film on the

strip, and ϕ_{j-1} and ϕ_j are the potential corresponding to the regions at the left and the right of the strip, respectively. The conditions on the derivatives are obtained by using mass conservation.

If the strips form an ordered array $X_j = jb$, with b being the distance between strip centers, the behavior of the third-sound excitations can be described by elementary methods. A simple band structure with alternating allowed and forbidden regions for the wave number was obtained in Ref. 33. There, we also compared the boundary conditions (2.2) to those occurring in a square-well electronic Kronig-Penney potential.

In this paper we consider the distance between strips to be random, specifying only the strip density n. (See Fig. 1.) Our treatment allows overlapping strip configurations. The initial conditions are similar to those used previously,[23,24,27]

$$\phi(x, t \leqq 0) = 0 \tag{2.3}$$

and

$$\frac{\partial \phi}{\partial t}(x, t=0) = f(x) , \tag{2.4}$$

for a given initial perturbation $f(x)$.

An alternative disordered substrate can be created by "roughening" some pieces of an otherwise smooth substrate. The effective speed of sound c_s in the pieces of the film on the roughened parts can be substantially smaller than that on the smooth substrate. These pieces of film therefore act as very efficient scatterers (indices of refraction $N = c/c_s$ as high as five for roughened Si have been reported[34]).

The rough regions may be distributed as a random array of strips similar to that in Fig. 1. We call these strips index-of-refraction (IR) scatterers. It is not difficult to include both possibilities for the scatterers (i.e., simultaneous changes in the thickness and speed of sound) in the formalism. The velocity potential satisfies a wave equation with speed of sound c on the unperturbed substrate and c_s on the strips, and the boundary conditions (2.2) must be satisfied.

B. Multiple-scattering formalism

The velocity potential can be written in terms of a Green's function as

$$\phi(x,t) = \int dx' \, G(x,t \mid x') f(x') . \tag{2.5}$$

The Green's function satisfies the differential equations

$$\left[\frac{\partial^2}{\partial x^2} - \frac{1}{c^2} \frac{\partial^2}{\partial t^2} \right] G(x,t \mid x') = 0 \tag{2.6a}$$

and

$$\left[\frac{\partial^2}{\partial x^2} - \frac{1}{c_s^2} \frac{\partial^2}{\partial t^2} \right] G(x,t \mid x') = 0 , \tag{2.6b}$$

outside and inside the strips, respectively, together with the same boundary conditions as ϕ [Eqs. (2.2)]. The initial conditions are

$$G(x, t \leqq 0 \mid x') = 0 \tag{2.7}$$

and

$$\frac{\partial G}{\partial t}(x, t=0 \mid x') = \delta(x - x') . \tag{2.8}$$

As in Ref. 27, it is convenient to introduce an operator notation in such a way that the matrix elements of the Green's operator $\hat{G}^{\pm}$ in a coordinate representation are

$$G_E^{\pm}(x \mid x') = \langle x \mid \hat{G}_E^{\pm} \mid x' \rangle . \tag{2.9}$$

Here, $G_E^{\pm}(x \mid x')$ are the Laplace transforms of the retarded and advanced solutions of Eq. (2.6):

$$G_E^{\pm}(x \mid x') = \int_0^{\infty} dt \, e^{i(\omega \pm i\epsilon)t} G^{\pm}(x,t \mid x') , \tag{2.10}$$

with $\epsilon \to 0$. In particular, the coordinate representation for the Green's operator in the absence of scatterers is

$$\langle x \mid \hat{G}_{E,0}^{\pm} \mid x' \rangle = - \left[(E \pm i\epsilon)^2 + c^2 \frac{\partial^2}{\partial x^2} \right]^{-1} \delta(x - x') . \tag{2.11}$$

In the wave-number representation we obtain

$$G_E^{\pm}(p \mid p') = \langle p \mid G_E^{\pm} \mid p' \rangle = \frac{1}{2\pi} \int dx \, dx' \, e^{-ipx} e^{ip'x'} G_E^{\pm}(x \mid x') . \tag{2.12}$$

If there are no scatterers present, $G_E^{\pm}(p \mid p') = G_{E,0}^{\pm}(p) \delta(p - p')$.

The multiple-scattering formalism can now be introduced in the usual manner.[26,27] If $\hat{G}_j$ is the Green's operator when there is only one strip present at X_j, we can first define a $\hat{T}_j$ operator whose matrix elements form the transition matrix for that single strip:

$$\hat{G}_{E,j}^{\pm} = \hat{G}_{E,0}^{\pm} + \hat{G}_{E,0}^{\pm} \hat{T}_j^{\pm}(E) \hat{G}_{E,0}^{\pm} . \tag{2.13}$$

To calculate the matrix elements of $\hat{T}_j$, we first define the ket vectors,

$$\mid \psi \rangle^{\pm} = \hat{G}_{E,j}^{\pm} \mid p \rangle , \tag{2.14}$$

with $\mid p \rangle$ being a momentum eigenstate. Then, the desired matrix elements are given by

$$\langle p \mid \hat{T}_j^{\pm}(E) \mid p_1 \rangle = [G_{E,0}^{\pm}(p)]^{-1} \langle p \mid \psi \rangle^{\pm} [G_{E,0}^{\pm}(p_1)]^{-1} - \delta(p - p_1) [G_{E,0}^{\pm}(p_1)]^{-1} . \tag{2.15}$$

With the definition

$$\langle p \mid \psi \rangle^{\pm} = (2\pi)^{-1/2} \int dx \, e^{-ipx} \langle x \mid \psi \rangle^{\pm} , \tag{2.16}$$

we can obtain a solution for our matrix elements by solving the differential equations

$$- \left[(E \pm i\epsilon)^2 + c^2 \frac{\partial^2}{\partial x^2} \right] \langle x \mid \psi \rangle_{A,C}^{\pm} = (2\pi)^{-1/2} e^{ip_1 x} \tag{2.17a}$$

and

$$-\left[(E\pm i\epsilon)^2+c_s^2\frac{\partial^2}{\partial x^2}\right]\langle x\mid\psi\rangle_B^{\pm}=(2\pi)^{-1/2}e^{ip_1x}\ , \quad (2.17b)$$

where A, B, and C denote, respectively, the regions $x<X_j-a$, $X_j-a<x<X_j+a$, and $X_j+a<x$. The boundary conditions are those in Eqs. (2.2). After a lengthy but straightforward calculation we obtain

$$\langle p\mid\hat{T}_j^{\pm}(E)\mid p_1\rangle=e^{i(p_1-p)X_j}\langle p\mid\hat{T}^{\pm}(E)\mid p_1\rangle\ , \quad (2.18)$$

where the location of the strips appears only in the exponential factor. The matrix elements $\langle p\mid\hat{T}^{\pm}(E)\mid p_1\rangle$ are given in Appendix A. They satisfy the identities

$$\langle p\mid\hat{T}^{\pm}(E)\mid p_1\rangle=\langle p\mid\hat{T}^{\mp}(E)\mid p_1\rangle^*\ , \quad (2.19a)$$

$$\langle p\mid\hat{T}^{\pm}(-E)\mid p_1\rangle=\langle p\mid\hat{T}^{\pm}(E)\mid p_1\rangle^*\ , \quad (2.19b)$$

$$\langle p\mid\hat{T}^{\pm}(E)\mid p\rangle=\langle -p\mid\hat{T}^{\pm}(E)\mid -p\rangle\ , \quad (2.19c)$$

$$\langle p\mid\hat{T}^{\pm}(E)\mid -p\rangle=\langle -p\mid\hat{T}^{\pm}(E)\mid p\rangle\ , \quad (2.19d)$$

and an optical relation,

$$\mathrm{Im}\langle p\mid\hat{T}^{\pm}(E)\mid p\rangle=\pm(\pi/2Ec)(\mid\langle p\mid\hat{T}^{\pm}\mid p\rangle\mid^2+\mid\langle p\mid\hat{T}^{\pm}\mid -p\rangle\mid^2)\ , \quad (2.20)$$

for $p=E/c$.

The N-strip ($N\to\infty$) Green's operator can be expressed in terms of an infinite series of individual $\hat{T}_i$ operators:

$$\hat{G}_E^{\pm}=\hat{G}_{E,0}^{\pm}+\sum_{i=1}^{N}\hat{G}_{E,0}^{\pm}\hat{T}_i^{\pm}(E)\hat{G}_{E,0}^{\pm}+\sum_{i\neq j}^{N}\hat{G}_{E,0}^{\pm}\hat{T}_i^{\pm}(E)\hat{G}_{E,0}^{\pm}\hat{T}_j^{\pm}(E)\hat{G}_{E,0}^{\pm}+\cdots\ , \quad (2.21)$$

where no two consecutive $\hat{T}_i$ operators can have the same label.

C. The averaged Green's function

Assuming the strips are randomly distributed, the Green's function averaged over the random locations of the scatterers (this spatial averaging is denoted by $\langle\cdots\rangle_{\mathrm{av}}$) is diagonal in the wave-number representation:

$$\langle\langle p\mid\hat{G}_E^{\pm}\mid p_1\rangle\rangle_{\mathrm{av}}=\delta(p-p_1)\langle G_{E\pm i\epsilon}^{\pm}(p)\rangle_{\mathrm{av}}=\delta(p-p_1)[c^2p^2-(E\pm i\epsilon)^2-\Sigma_p^{\pm}(E)]^{-1}\ . \quad (2.22)$$

The lowest-order diagrams for the self-energy $\Sigma_p^{\pm}(E)=\gamma_p(E)\pm i\sigma_p(E)$ are shown in Fig. 2. The rules for their evaluation are identical to those in Refs. 27 and 35. The leading contribution for low densities yields

$$\Sigma_p^{\pm}(E)\simeq 2\pi n\langle p\mid\hat{T}^{\pm}(E)\mid p\rangle\ . \quad (2.23)$$

The Laplace components of the velocity potential at (x,t) generated by the point source at x' are obtained via a Fourier transform of Eq. (2.22):

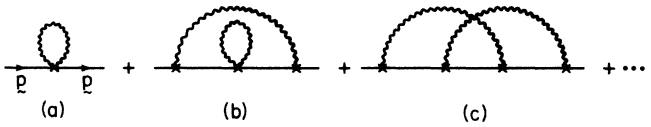

FIG. 2. Self-energy diagrams. The $\hat{T}$ operators are denoted by crosses and the restrictions on the sums in Eq. (2.21) forbid diagrams containing the element ⌒.

$$G_E^{+}(x,x')=\frac{1}{2\pi}\int_{-\infty}^{\infty}dp\frac{e^{ip(x-x')}}{c^2p^2-E^2-\gamma_p(E)-i\sigma_p(E)}\ . \quad (2.24)$$

Evaluating the integral in Eq. (2.24), it is possible to define a renormalized speed of sound $\tilde{c}$ and an effective attenuation parameter $\tilde{\Gamma}$. This attenuation is due to destructive interference effects originating in the scatterers. The integral can be approximately evaluated by substituting E/c for p in the self-energy terms, whose coefficients are small and thus become important only in the neighborhood of $p=\pm E/c$. (This would not be the case at low frequencies if there is a high density of strong scatterers, but then higher-order diagrams must be included.) Defining $\eta=2Ea/c$, $r=h_2/h_1$, and

$$D(x)=x[4x^2+(x^2-1)^2\sin^2(\eta N)]^{-1}\ ,$$

we obtain, for the renormalized speed of sound $\tilde{c}$,

$$\tilde{c}^2(E)\simeq c^2(1-4na\eta^{-1}D(rN)\{(rN+1)^2\sin[\eta(N-1)]+(rN-1)^2\sin[\eta(N+1)]\})\ , \quad (2.25)$$

with its long-wavelength ($\eta\ll 1$) limit

$$\tilde{c}\to c[1-(na/r)(r^2N^2-2r+1)]\ .$$

The effective attenuation $\tilde{\Gamma}(E)\simeq E^{-1}\sigma_p(E)$, where $p=E/c$, is

$$\tilde{\Gamma}(E)\simeq 2nc(1-D(rN)\{(rN+1)^2\cos[\eta(N-1)]-(rN-1)^2\cos[\eta(N+1)]\})\ , \quad (2.26)$$

with its long-wavelength limit

$$\tilde{\Gamma}\to(n/2)cr^{-2}\eta^2(r^4N^4-2r^3N^2+2r^2-2r+1)\ .$$

The corresponding attenuation length is $L_a(E)=2c\tilde{\Gamma}^{-1}(E)$.

We note that r and N always appear in the combination rN, except in the arguments of the circular functions. These arguments are modified because of the phase lag caused by an index of refraction different from unity, an effect that is not present in the vDW scatterer case. The variables E, a, and c appear in the combination $\eta=2Ea/c$ [except for the factor na in Eq. (2.25)], which is 2π times the ratio between the strip width and the wavelength $\lambda=2\pi c/E$.

Equations (2.25) and (2.26) show some interesting quali-

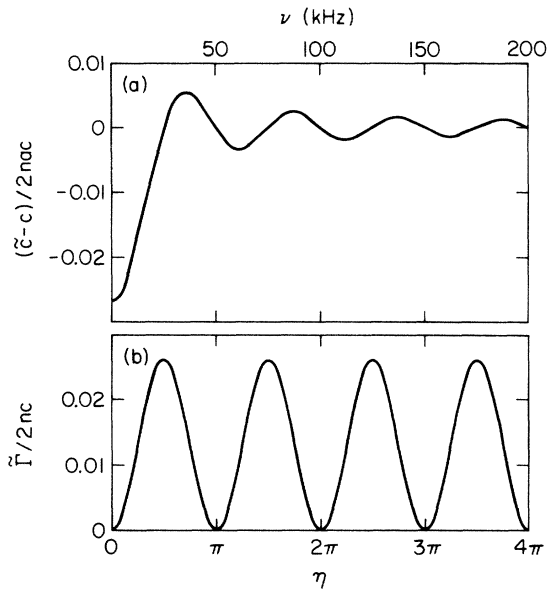

FIG. 3. (a) Renormalized speed of sound and (b) effective attenuation for van der Waals scatterers with $r=1.26$. In the lower scale we only specify $\eta=2Ea/c$, while in the upper scale we give the values of $\nu=E/2\pi$ corresponding to $a=0.005$ cm and $c=10^3$ cm/sec.

tative features that are not evident from the long-wavelength limit studied in Ref. 23. The renormalized speed of sound and the attenuation parameter are plotted in Fig. 3 for vDW scatterers in the case $r=1.26$, corresponding to a ratio of about two between the van der Waals constants. We have chosen a relatively high strip density ($n=40$ strips/cm). [The magnitudes we actually graph are $(\tilde{c}-c)/2\pi ac$ and $\tilde{\Gamma}/2nc$, since, except for negligible corrections, they are functions of η and r alone.] The renormalized speed of sound for IR scatterers is graphed in Fig. 4 for several values of the index. The values for c have been taken to be approximately those corresponding to clean Si substrates.[34] The curves for

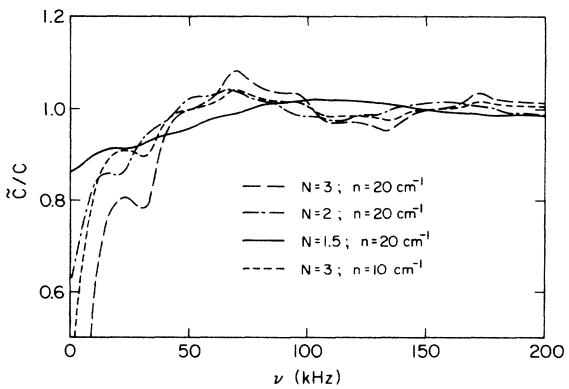

FIG. 4. Renormalized speed of sound for index of refraction scatterers. The unrenormalized speeds of sound c correspond to experimental values on smooth substrates (see text). The frequency ν is $\nu=E/2\pi$.

$N=3$ correspond to $c=2040$ cm/sec (film thickness of about 7 layers), that for $N=2$ corresponds to $c=900$ cm/sec (film thickness of about 13 layers), and that for $N=1.5$ corresponds to $c=750$ cm/sec (film thickness of about 16 layers). In all figures we take the strip width to be $2a=10^{-2}$ cm.

We note the following:

(1) At low frequencies the waves are slowed down by the scatterers. However, as we increase the frequency, $\tilde{c}$ oscillates between values higher and lower than c, becoming more and more sensitive to the presence of the strips. For relatively weak scatterers $\tilde{c}$ is not very different from the speed of sound on the original substrate, but for stronger scatterers the deviations are quite large at low frequencies. This can be seen to occur in the $N=3$ curves in Fig. 4 at frequencies $\nu \lesssim 15$ kHz if $n=20$ cm^{-1} and at $\nu \lesssim 5$ kHz if $n=10$ cm^{-1}. Indeed, under those conditions the approximation of using only the lowest-order diagram to evaluate the self-energy does not yield accurate results, and higher-order diagrams must be included. We believe that the contribution of these diagrams will be to decrease the difference between c and $\tilde{c}$ at low frequencies. It is not difficult to verify, taking the limit $E\to 0$, that in the vDW case the contributions of the first and third diagrams in Fig. 2 have opposite signs, while the second diagram is irrelevant (the IR case is more difficult to treat).

(2) For vDW scatterers, the randomness-induced attenuation is a periodic function (approximately a squared sine), which vanishes when the strip width is an integer multiple of the half-wavelength ($2a=j\lambda/2$, for $j=1,2,\ldots$). We expect resonant transmission to occur at these wavelengths. This is confirmed in Sec. III, where the localization properties of third-sound waves are discussed. An analogous effect is found if we consider the transmission coefficient for a third-sound wave incident in an *ordered* collection of parallel, identical strips: If the relations between strip width and excitation wavelength is $2a=j\lambda/2$, the transmission coefficient for the whole array becomes unity.[33] The attenuation is also proportional to strip density. If $n=40$ strips/cm, $r=1.26$, and $c=10^3$ cm/sec, then $\tilde{\Gamma}\simeq 2\times 10^3$ sec^{-1}. This is much larger than a value reported for intrinsic dissipation[31] ($\Gamma\simeq 1$ sec^{-1}). Similar results are obtained in the IR case. Even if the intrinsic dissipation is substantially increased in the roughened regions, it does not seem probable that Γ will become of the order of $\tilde{\Gamma}$. Therefore, it is reasonable to neglect intrinsic dissipation completely in the problems we are considering here, except inasmuch as it determines the lifetime of the localized excitations. An experimentalist can easily verify that he is measuring $\tilde{\Gamma}$ and not Γ by performing a measurement of Γ in a uniformly roughened substrate. We remark that, for the IR scatterers, the attenuation length obtained from the average Green's function is not always physically meaningful. We will return to this point in Sec. III D.

III. LOCALIZATION OF THIRD-SOUND WAVES

In this section we analyze the localization of the third-sound waves in the random substrate. We first define the intensity propagator and derive the kinetic equation it satisfies. We then solve this kinetic equation and use the

self-consistent approximation of Vollhardt and Wölfle[28] to calculate the frequency-dependent diffusion coefficient and the localization length.

A. Kinetic equation

The analysis of the localization effects involves[36,37] the average of the squared Green's function, $G^2(x,t\,|\,x')$, which is proportional to the energy density at position x and time t due to a disturbance created at the source point x' at $t=0$. It is convenient to rewrite its Laplace transform as follows:

$$P_\omega(x\,|\,x')=\int_0^\infty dt\,\exp[i(\omega+i\epsilon)t]G^2(x,t\,|\,x') = \int_{-\infty}^{\infty}\frac{dE}{2\pi}G^+_{E+\omega/2}(x\,|\,x')G^-_{E-\omega/2}(x\,|\,x') = \int_{-\infty}^{\infty}\frac{dE}{2\pi}P_{E,\omega}(x\,|\,x')\,. \tag{3.1}$$

In using the convolution property of the Laplace transform we have introduced a new frequency E, which can be related to the microscopic fluctuations whose superposition at a given time yields the total $P(x,t\,|\,x')$. The external frequency ω is related to the temporal behavior of the "envelope" $P(x,t\,|\,x')$. The internal frequency E is the one relevant to any "microscopic" experiment probing the individual excitations of the system.

The intensity propagator $\langle P_E(k,\omega)\rangle_{\rm av}$ is the k and ω Fourier component of the average intensity resulting from the E Fourier component of a pulse excited at the origin:

$$\langle P_E(k,\omega)\rangle_{\rm av}=\int d(x-x')\exp[-ik(x-x')] \times\langle P_{E,\omega}(x\,|\,x')\rangle_{\rm av}\,. \tag{3.2}$$

We note that the T matrix is not symmetric and $G^\pm_E(x\,|\,x')\neq G^\pm_E(x'\,|\,x)$. However, because of the low scatterer density, we will evaluate the relevant vertices at the poles $p=\pm E/c$ of $G_{E,0}(p)$. Using the symmetry of the pole locations and the properties (2.19) of the T matrix, it is easy to see that the results do not depend on the ordering of the spatial arguments in $G^-_E(x\,|\,x')$, which we have substituted by $G^-_E(x'\,|\,x)$ in the developing the formalism for $\langle P_{E,\omega}(x\,|\,x')\rangle_{\rm av}$. This allows us to keep a closer analogy to the electron-localization problem. Using the notation introduced in Eq. (2.12), we can write

$$\langle P_E(k,\omega)\rangle_{\rm av}=l^{-1}\int dp\,dp_1\langle\langle p_+\,|\,\hat G^+_{E+}\,|\,p_{1+}\rangle \times\langle p_{1-}\,|\,\hat G^-_{E-}\,|\,p_-\rangle\rangle_{\rm av}\,, \tag{3.3}$$

where

$$p_\pm=p\pm k/2\,, \tag{3.4a}$$

$$E_\pm=E\pm\omega/2\,, \tag{3.4b}$$

and l is the total length of the system, assumed to be much larger than any other relevant lengths (except for l_i, which, as we have seen, can be taken to be infinite for all practical purposes). The averaged product of the two Green's functions in Eq. (3.3) can be represented in terms of the diagrams shown in Fig. 5.[28,35] The corresponding analytical expression is

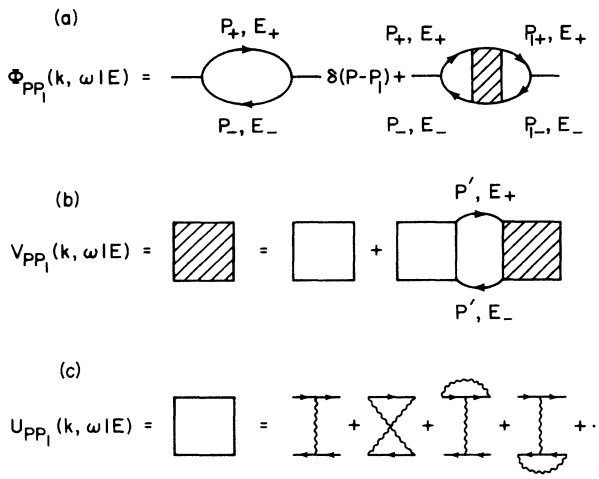

FIG. 5. (a) The integrand Φ in the intensity propagator can be expressed in terms of a vertex function V. (b) The irreducible components of V can be separated to form an irreducible vertex function U. (c) The lowest-order irreducible diagrams. (An irreducible diagram is one which cannot be split into two disjoint parts by vertically cutting both solid lines.)

$$\langle\langle p_+\,|\,\hat G^+_{E+}\,|\,p_{1+}\rangle\langle p_{1-}\,|\,\hat G^-_{E-}\,|\,p_-\rangle\rangle_{\rm av}=(l/2\pi)\langle G(p_+,E_++i\epsilon)\rangle_{\rm av}\langle G(p_-,E_--i\epsilon)\rangle_{\rm av} \times[\delta(p-p_1)+V_{pp_1}(k,\omega\,|\,E)\langle G(p_{1+},E_++i\epsilon)\rangle_{\rm av}\langle G(p_{1-},E_--i\epsilon)\rangle_{\rm av}]\,. \tag{3.5}$$

The four-point vertex function $V_{pp_1}(k,\omega\,|\,E)$ contains both reducible and irreducible diagrams. It is convenient to define the irreducible four-point vertex function U_{pp_1}, which is related to V_{pp_1}, by [See Fig. 5(b)]

$$V_{pp_1}(k,\omega\,|\,E)=U_{pp_1}(k,\omega\,|\,E)+\int dp'U_{pp'}(k,\omega\,|\,E)\langle G(p',E_++i\epsilon)\rangle_{\rm av}\langle G(p',E_--i\epsilon)\rangle_{\rm av}V_{p'p_1}(k,\omega\,|\,E)\,. \tag{3.6}$$

The first few diagrams that contribute to U_{pp_1} are shown in Fig. 5(c). Equation (3.5) can now be integrated over p_1 to yield

$$\Phi_p(k,\omega\,|\,E)\equiv\int dp_1\langle\langle p_+\,|\,\hat G^+_{E+}\,|\,p_{1+}\rangle\langle p_{1-}\,|\,\hat G^-_{E-}\,|\,p_-\rangle\rangle_{\rm av} =\langle G(p_+,E_++i\epsilon)\rangle_{\rm av}\langle G(p_-,E_--i\epsilon)\rangle_{\rm av}\left[1+\int dp_2U_{pp_2}(k,\omega\,|\,E)\Phi_{p_2}(k,\omega\,|\,E)\right]\,. \tag{3.7}$$

The function Φ_p, related to the intensity propagator by

$$\langle P_E(k,\omega)\rangle_{\rm av}=(2\pi)^{-1}\int dp\,\Phi_p(k,\omega\,|\,E)\,, \tag{3.8}$$

can be shown to satisfy a generalized Boltzmann equation. Defining

$$\Delta\langle G(p)\rangle_{\rm av}\equiv\langle G(p_+,E_++i\epsilon)\rangle_{\rm av}-\langle G(p_-,E_--i\epsilon)\rangle_{\rm av}\,, \tag{3.9}$$

and using Eq. (2.22), we obtain

$$[2E\omega-2c^2kp+\Sigma_{p+}^{+}(E+)-\Sigma_{p-}^{-}(E_-)]\Phi_p(k,\omega\,|\,E)=\Delta\langle G(p)\rangle_{\rm av}\left[1+\int dp_2 U_{pp_2}(k,\omega\,|\,E)\Phi_{p_2}(k,\omega\,|\,E)\right]\,. \tag{3.10}$$

A considerable simplification ensues if we note that, for small k and ω, and a low density of scatterers, we can use the approximation

$$\Delta\langle G(p)\rangle_{\rm av}\simeq 2i\pi\tilde{c}^{-2}\delta(p^2-(E/\tilde{c})^2)\,. \tag{3.11}$$

B. The ladder approximation

We solve Eq. (3.10) to lowest order in the density by keeping only the first diagram in Fig. 5(c). Under these conditions, the irreducible four-point vertex function is given by

$$U^{B}_{pp_2}(k,\omega\,|\,E)=2\pi n\langle p_+\,|\,\hat{T}^{+}(E_+)\,|\,p_{2+}\rangle\langle p_{2-}\,|\,\hat{T}^{-}(E_-)\,|\,p_-\rangle\,. \tag{3.12}$$

The superscript B in Eq. (3.12) stands for Boltzmann: To this order the kinetic equation has the form of a Boltzmann equation. Neglecting the k and ω dependence in $U^{B}_{pp_2}$ and using Eq. (3.11) yields[27]

$$[2E\omega-2\tilde{c}^2kp+2i\sigma_p(E)]\Phi_p(k,\omega\,|\,E)=(2i\pi/c^2)\delta(p^2-(E/\tilde{c})^2)\times\left[1+2\pi n\int dp_2\langle p\,|\,\hat{T}^{+}(E)\,|\,p_2\rangle\langle p_2\,|\,\hat{T}^{-}(E)\,|\,p\rangle\Phi_{p_2}(k,\omega\,|\,E)\right]\,. \tag{3.13}$$

The k dependence of the real part of the self-energies has been kept to the lowest order. This renormalizes the speed of sound appearing on the second term of the left-hand side.

Writing the solution Φ_p in the form

$$\Phi_p(k,\omega\,|\,E)=\delta(p^2-(E/\tilde{c})^2)\psi_{\hat{p}}(k,\omega\,|\,E)\,, \tag{3.14}$$

we note that $\psi_{\hat{p}}$ is evaluated at only two points as a function of $\hat{p}$. Let $\psi_{\hat{p}}=\psi_+$ if $pk>0$ and $\psi_{\hat{p}}=\psi_-$ if $pk<0$; define

$$\chi=(\pi^2ni/E\tilde{c})\,|\,\langle p\,|\,\hat{T}^{+}\,|\,-p\rangle\,|^2\,, \tag{3.15}$$

with the matrix element evaluated at $p=E/\tilde{c}$. With this notation, the substitution of Eq. (3.14) into Eq. (3.13) leads to the following pair of equations for ψ_+ and ψ_-:

$$(E\omega-\tilde{c}^2\,|\,k\,|\,|\,p\,|+\chi)\psi_+-\chi\psi_-=i\pi/\tilde{c}^2 \tag{3.16a}$$

and

$$(E\omega+\tilde{c}^2\,|\,k\,|\,|\,p\,|+\chi)\psi_--\chi\psi_+=i\pi/\tilde{c}^2\,. \tag{3.16b}$$

Here the optical relation, Eq. (2.20), has been used, with one modification: For self-consistency, we have replaced c by the renormalized speed of sound $\tilde{c}$.

For small $|\,k\,|$ and ω, Eqs. (3.16) yield

$$\psi_+=\psi_-=(\pi/\tilde{c}^2E)[-i\omega+D_B(E)k^2]^{-1}\,, \tag{3.17}$$

where the "Boltzmann" diffusion coefficient $D_B(E)$ is

$$D_B(E)=\left[\frac{\tilde{c}}{2n}\right]\left[\frac{4r^2N^2+(r^2N^2-1)^2\sin^2(\tilde{\eta}N)}{(r^2N^2-1)^2\sin^2(\tilde{\eta}N)}\right]\,. \tag{3.18}$$

Here, $\tilde{\eta}=2Ea/\tilde{c}$. Equation (3.17) is a valid representation for

$$|\,k\,|<2\,|\,\chi\,|/(\tilde{c}E)\sim\tilde{c}D_B^{-1}(E)\equiv q_0\,.$$

Here, q_0 is a wave-number cutoff. Naturally, $D_B(E)\to\infty$ if $r,N\to 1$. The diffusion coefficient also diverges when $N\tilde{\eta}=j\pi$, for all integers j. In this case we expect resonant transmission instead of localization. This is confirmed below.

Using Eq. (3.17) in conjunction with Eq. (3.8), we find that the intensity propagator exhibits a diffusive hydrodynamic pole,

$$\langle P_E(k,\omega)\rangle_{\rm av}=\frac{1}{2\tilde{c}^3}\left[\frac{\tilde{c}}{E}\right]^2\frac{1}{-i\omega+D_B(E)k^2}\,. \tag{3.19}$$

C. Maximally crossed diagrams

Since localization is a result of wave interference, the relevant information about localization must be contained in the irreducible four-point vertex function U_{pp_1}: this is the function that may show a singular behavior. We next express the diffusion coefficient $D(E,\omega)$ in terms of U_{pp_1}. $D(E,\omega)$ depends on both internal and external frequencies. Its behavior as $\omega\to 0$ determines whether or not the excitation is localized. Indeed, U_{pp_1} turns out to diverge when $\omega\to 0$, but is regular when $k\to 0$.

We define the auxiliary functions

$$\Xi(k,\omega\,|\,E)=\int dp\,\Phi_p(k,\omega\,|\,E) \tag{3.20}$$

and

$$\Xi_I(k,\omega\,|\,E)=2\int dp\,p\Phi(k,\omega\,|\,E)\ . \tag{3.21}$$

Integrating Eq. (3.10) over p, and using a Ward identity that expresses energy conservation, we find that these functions satisfy the equation,

$$2E\omega\Xi(k,\omega\,|\,E)-c^2k\Xi_I(k,\omega\,|\,E)=2i\pi/\tilde{c}E\ . \tag{3.22}$$

If we multiply Eq. (3.10) times $2p$ and then integrate over p, we find, after some algebra, a second relation between Ξ and Ξ_I which is valid for small values of ω and k:

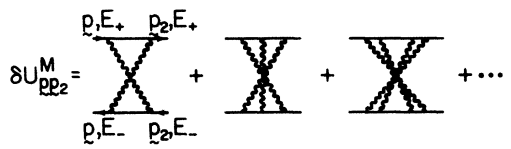

FIG. 6. Maximally crossed diagrams.

$$\left[\int dp\,p^2[\Sigma_p^+(E)-\Sigma_p^-(E)]\Delta G(p)-\int dp\,dp_2\Delta G(p)\Delta G(p_2)pp_2U_{pp_2}\right]\Xi_I(k,\omega\,|\,E)=\pi i(E/\tilde{c})^3k\Xi(k,\omega\,|\,E)\ . \tag{3.23}$$

Using Eq. (3.23), we can eliminate the function Ξ_I from (3.22) to obtain the following equation for the intensity propagator:

$$\langle P_E(k,\omega)\rangle_{\rm av}=(2\pi)^{-1}\Xi(k,\omega\,|\,E)=(2\tilde{c}E^2)^{-1}[-i\omega+D(E,\omega)k^2]^{-1}\ , \tag{3.24}$$

where the diffusion coefficient $D(E,\omega)$ is given by

$$D(E,\omega)=4\pi E^2\tilde{c}^{-1}\left[\int dp\,dp_2\Delta G(p)\Delta G(p_2)pp_2U_{pp_2}-\int dp\,p^2[\Sigma_p^+(E)-\Sigma_p^-(E)]\Delta G(p)\right]^{-1}\ . \tag{3.25}$$

From this equation it follows that

$$D^{-1}(E,\omega)=D_B^{-1}(E)+(\tilde{c}/4\pi E^2)\int dp\,dp_2\,pp_2\,\Delta G(p)\Delta G(p_2)\delta U_{pp_2}(0,\omega\,|\,E)\ , \tag{3.26}$$

where

$$\delta U_{pp_2}(0,\omega\,|\,E)=U_{pp_2}(0,\omega\,|\,E)-U^B_{pp_2}(0,\omega\,|\,E)\ . \tag{3.27}$$

We have taken $k=0$ in δU_{pp_2} since it can be explicitly verified that the maximally crossed diagrams represent nonsingular functions of k. We have again used a self-consistency argument to substitute $\tilde{c}$ for c.

We must evaluate the corrections to the Boltzmann diffusion coefficient $D_B(E)$ due to the diagrams in δU_{pp_2}. One particular subset of these, that of the maximally crossed diagrams shown in Fig. 6, is essential for an analysis of localization.[28] These diagrams can be resummed by rotating the "hole" line in Fig. 6, 180°, and using spatial homogeneity to reverse the momenta on that line. An equation pair formally similar to Eqs. (3.16) ensues. Finally, we obtain, for small ω and $q=p+p_2$, that the contribution $\delta U^M_{pp_2}$ of the maximally crossed diagrams is

$$\delta U^M_{pp_2}\simeq[\tilde{c}\sigma^2(E)/\pi][-i\omega+D_B(E)q^2]^{-1}\ , \tag{3.28}$$

where $\sigma(E)$ is the imaginary part of the self-energy evaluated at $p=E/\tilde{c}$. This contribution has again the form of a hydrodynamic diffusive pole. When substituted into Eq. (3.26) it yields

$$D^{-1}(E,\omega)=D_B^{-1}(E)+\frac{\sigma(E)}{\pi\tilde{c}E}\int_0^{q_0}\frac{dq}{-i\omega+D_B(E)q^2}\ . \tag{3.29}$$

Here we have introduced the hydrodynamic cutoff q_0 discussed above. The necessity for a finite cutoff arises from the nondiffusive behavior of the excitation for lengths smaller than q_0^{-1}; at these short lengths there is effectively ballistic propagation of the excitations.

D. Self-consistent theory: The localization length

In the self-consistent theory of localization, we replace the low-density hydrodynamic pole appearing in the perturbative result (3.29) by an exact hydrodynamic pole.[28] In practice, this means substituting $D(E,\omega)$ for the Boltzmann diffusion coefficient D_B. Thus, $D(E,\omega)$ solves the following equation:

$$\frac{1}{D(E,\omega)}=\frac{1}{D_B(E)}+\frac{\sigma(E)}{\pi\tilde{c}E}\int_0^{q_0}\frac{dq}{-i\omega+D(E,\omega)q^2}\ . \tag{3.30}$$

Here, $D_B(E)$ is given by Eq. (3.18), and $\sigma(E)$ can be obtained from Eqs. (2.23) and (A1):

$$\sigma(E)=D_B^{-1}(E)E\tilde{c}^2(1+rN(N^2r^2-1)^{-2}\sin^{-2}(\eta N)\{4rN-(Nr+1)^2\cos[\eta(N-1)]+(Nr-1)^2\cos[\eta(N+1)]\})\ . \tag{3.31}$$

Upon integration, Eq. (3.30) yields the transcendental equation

$$D(E,\omega)=D_B(E)\left\{1-\frac{\sigma(E)i}{\pi\tilde{c}E}\left[\frac{D(E,\omega)}{i\omega}\right]^{1/2}\arctan\left[i\left[\frac{D(E,\omega)}{i\omega}\right]^{1/2}q_0\right]\right\}\ . \tag{3.32}$$

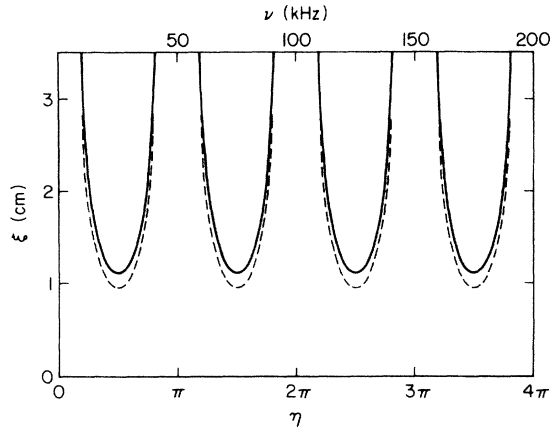

FIG. 7. Localization (solid line) and attenuation (dashed line) lengths for vDW scatterers with $r=1.26$. The horizontal scales are identical to those in Fig 3.

It is easy to see that the solution to Eq. (3.32) for $\omega\rightarrow 0$ is given by

$$D(E,\omega\rightarrow 0)=-i\omega\xi^2(E)+O(\omega^2)\ . \tag{3.33}$$

Here, $\xi(E)$ is the frequency-dependent localization length which satisfies the equation

$$\sigma(E)\xi(E)\arctan[q_0(E)\xi(E)]=\pi E\tilde{c}\ . \tag{3.34}$$

Note that, taking $\arctan(q_0\xi)=\pi/2$, our result (3.34) yields $\xi=L_a$, where L_a is the attenuation length obtained from Eq. (2.26). This approximation turns out to be reasonable for vDW scatterers, for which $q_0\xi\approx 4.5$ for all experimental values. It is not reasonable for IR scatterers, for which $q_0\xi$ oscillates as a function of E and even vanishes at certain frequencies.

Equation (3.34) is easy to solve numerically. We first consider vDW scatterers. The lengths ξ and L_a are shown in Fig. 7 for $r=1.26$ and 40 strips/cm. They are periodic functions of the frequency and $\xi\simeq 1.15L_a$ everywhere. The most interesting features in Fig. 8 are the wide transmission resonances, which occur at values of the third-sound wavelength $\lambda=c/\nu$ that satisfy $j\lambda/2=2a$, for $j=1,2,3,\ldots$. These values correspond to the eigenfrequencies of an isolated piece of film located on a strip of width $2a$. For these frequencies the transmission coefficient for an isolated scatterer is unity; since the scatterers are identical, it follows that the random substrate is transparent to the third-sound excitation.

The resonances are obtained only if we perform an exact evaluation of the T matrix. A long-wavelength approximation to the T matrix, as in Ref. 23, or a white-noise representation of the scattering, as in Ref. 24, do not give any information about resonant behavior.

It is important to remark that reasonably short localization lengths ($\xi\sim 1$ or 2 cm) can be obtained at frequencies as low as 20 kHz, a smaller value than that predicted in Ref. 23, where an algebraic mistake was made. There Eq. (20) should read

$$\xi(E)\simeq\frac{1}{n}\left[\frac{\tilde{c}}{Ea}\right]^2\frac{(h_1h_2)^2(h_2+1)^2}{(h_1^2-h_2^2)^2(h_2^2+1)}\ , \tag{3.35}$$

and the numerical value we gave for the frequencies corresponds to rad/sec and not to Hz.

Near the resonances, the localization length can be easily shown to diverge as $|\nu-\nu_j|^{-2}$, where ν_j is the frequency corresponding to the jth resonance. Defining the resonance width $\delta\nu$ as the length of the neighborhood of ν_j such that $\xi(\nu)>\xi_0$ if $|\nu-\nu_j|<\delta\nu$, we obtain

$$\delta\nu\sim\tilde{c}r(2\pi a\,|r-1|)^{-1}[(r^2+1)n\xi_0]^{-1/2}\ . \tag{3.36}$$

Here, ξ_0 is a length that may be arbitrarily chosen. The width of the resonances is such that they can be considered truly "pass" bands. The resonances become sharper if r is increased.

Next we discuss the more complicated case of IR scatterers. The different effective speed of sound on the strips generates a phase change that is the source for a richer structure in the localization length. We plot $\xi(E)$ and $L_a(E)$ in Figs. 8–10 for several values of the index of refraction and $n=20$ strips/cm. The unrenormalized speeds of sound and the indices of refraction are again approximately those obtained by Smith and Hallock using Si

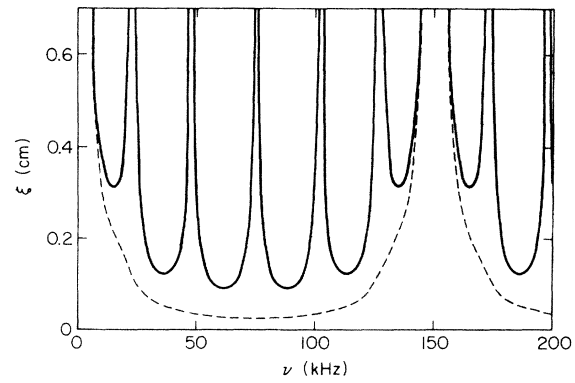

FIG. 8. Localization (solid line) and attenuation (dashed line) lengths for IR scatterers with $N=1.5$ and $c=750$ cm/sec.

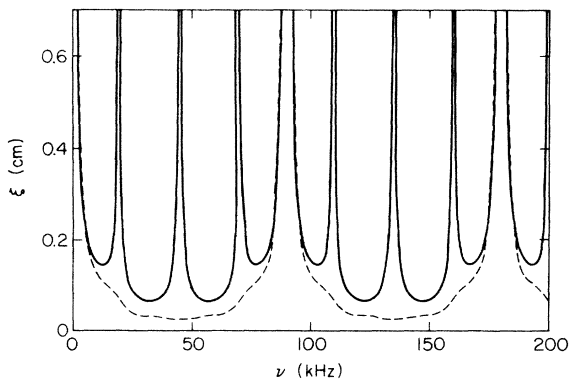

FIG. 9. Localization (solid line) and attenuation (dashed line) lengths for IR scatterers with $N=2$ and $c=900$ cm/sec.

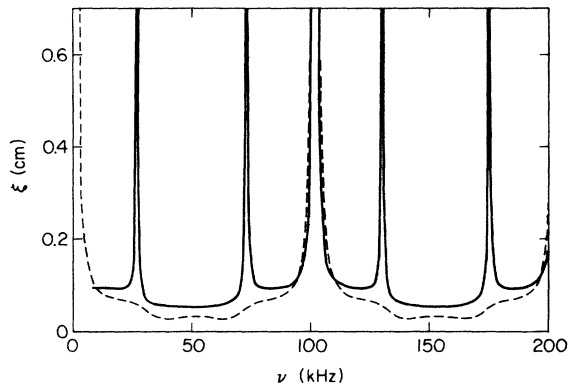

FIG. 10. Localization (solid line) and attenuation (dashed line) lengths for IR scatterers with $N=3$ and $c=2040$ cm/sec.

substrates.[34] We observe the following:

(1) All the resonances occur at values of the frequency such that the wavelength $\lambda_s=c_s/\nu$ for the third-sound on the strip satisfies

$$j\lambda_s/2=2a\ , \tag{3.37}$$

for $j=1,2,3,\ldots$.

(2) There are two types of resonances. At the thinner ones (type I) the localization length diverges as $\xi(\nu)\sim|\nu-\nu_j|^{-1}$, while at the wider ones (type II), it diverges as $\xi(\nu)\sim|\nu-\nu_j|^{-2}$. The typical width of a type-II resonance is

$$\delta\nu_{\rm II}\sim 0.2\tilde{c}(a\,|N^2-1|)^{-1}(n\xi_0)^{-1/2}\ , \tag{3.38}$$

while type-I resonances have a width $\delta\nu_{\rm I}\sim A_j(n\xi_0)^{-1/2}\delta\nu_{\rm II}$, where A_j is a coefficient of the order of one, whose value depends on the particular resonance.

(3) For a type-II resonance to occur, N must be a rational number; if $N=P/Q$, the following condition must be satisfied, in addition to Eq. (3.37):

$$k\lambda_s=4a/m\ , \tag{3.39}$$

where m is the integer appearing in the denominator that results from the reduction of the fraction $(P-Q)/2P$ to its lowest terms, and $k=1,2,3,\ldots$. It is easy to see that $m=6$ in case (a), $m=4$ in case (b), and $m=3$ in case (c).

(4) Experimentally, it is impossible to fix N to be a rational number but we expect that a $|\nu-\nu_j|^{-2}$ behavior will be observed whenever Eq. (3.39) is approximately satisfied. For irrational indices of refraction, however, the $|\nu-\nu_j|^{-2}$ behavior will cross over to a $|\nu-\nu_j|^{-1}$ divergence sufficiently close to the resonance.

The attenuation length is considerably shorter than the localization length (except near the type-II resonances) and does not show type-I resonances. This last result will be shown below to be an artifact of the averaging procedure.

Using the formulas in Appendix A, we find that the matrix elements $\langle p|\hat{T}^+|p\rangle$ and $\langle p|\hat{T}^+|-p\rangle$ evaluated at $p=E/c$ vanish at type-II resonances (as well as for the vDW scatterers), while for type-I resonances $\langle p|\hat{T}^+|-p\rangle=0$ but

$$\langle p|\hat{T}^+|p\rangle=(Eci/\pi)[1-(-1)^j\exp(-2iEa/c)]\ .$$

Although the ratio between the transmitted and incident amplitudes is unity for type-II resonances, it is

$$F/A=(-1)^j\exp(-2iEa/c) \tag{3.40}$$

for type-I resonances. We conclude that the excitation does not interact at all with the scatterers when the frequency is at a type-II resonance: neither the amplitude not the phase are modified. At type-I resonances there is a phase change even if the transmission coefficient is unity.

To understand the reason for the behavior we have found for the attenuation length, we consider the nature of the configurational average. Since the number of strips between the source and the detector depends on the particular element of the ensemble of substrates we consider, the total phase lag varies from element to element. Thus, the spatial average involves a sum over random phases, and we conclude that although there is resonant transmission for all members of the ensemble, the propagation on the "average" substrate is strongly attenuated. This unphysical behavior is due to the interactions between different systems in our ensemble or configurational average. For the same reason, we conclude that our value for L_a underestimates the real attenuation length for a given experimental system, even far from the resonances. However, it becomes unreasonable only when there is none or very little destructive forward-wave interference on each element of the ensemble, a condition that occurs in the neighborhood of type-I resonances.

The localization of the excitations is due to coherent backscattering. The calculation for ξ, involving the average of the squared Green's functions, is free of the problem of artificial phase cancellations. A discussion of the relation between ξ and L_a for the case of an electron in a weakly disordered lattice was given by Thouless.[38] Lu, Nelkin, and Arita dealt with the same problem for a glass-like disordered elastic chain.[39]

It should be easy to distinguish experimentally between a localized excitation and one that is merely attenuated. A detector located at a distance $d_2\gg\xi$ from the source (see Fig. 1) will not record anything in any case, and will at most give an upper bound for ξ (or L_a). However, another detector, located at a distance $d_1<\xi$ from the source will be able to detect thickness fluctuations in both cases. A clear signature of the occurrence of a localized excitation is its permanence. If the source is stopped at $t=0$ and the detector at d_1 does not record variations in thickness at times later than $\tau=d_1/\tilde{c}$, the experimentalist is observing an excitation that is simply attenuated. Since the intrinsic dissipation is expected to be small a localized excitation will remain relatively unattenuated for times $t>\tau$, and up to $t\sim\Gamma^{-1}$.

IV. CONCLUSION

A detailed analysis of Anderson localization of third-sound waves on a random substrate has been given. We found that transmission resonances occur at a discrete set

of frequencies; they correspond to a set of measure zero of extended states in the disordered system. Far from the resonances, the localization length can be very short especially for IR scatterers. We believe that, although the excitations are mostly confined to a small region containing only a few scatterers, their tails should be able to sense the disorder at distances beyond ξ. As we move toward the resonances, the localization weakens continuously, until the excitations can be considered to be essentially extended sufficiently close to the resonances. For typical values of the experimental parameters, the various "localization regimes" should be readily observable with present-day techniques. Due to the simplicitly of the system, we expect that the analysis of the experimental data can be made following closely the proposed theoretical model.

Three factors not considered in the theory and which could affect the results of an experiment (although not substantially, we believe) are as follows:

(1) Microscopic differences between the scatterers: Even if the strips can be manufactured in such a way that they are macroscopically identical, microscopic deviations from regularity may cause a lowering of the resonance peaks.

(2) Higher-order terms in the diagrammatic expansions: They may modify our detailed predictions, especially if the density of scatterers (or their strength) is high.

(3) Surface tension effects: They may become important at high frequencies if the amplitudes are not kept small.

It is not difficult to create and control a uniform flow in a superfluid helium film. It would be interesting to study what the effects (if any) of such a flow would be on the localization of the third-sound waves.

ACKNOWLEDGMENTS

We wish to express our acknowledgment to R. B. Hallock for suggesting the roughened strips as possible scatterers and for providing us with data prior to publication. We also thank Scott Cohen for some useful comments. This work was supported by the National Science Foundation under Grant No. DMR-83-09449, and a grant from the SOHIO Oil Company.

APPENDIX A: THE FULL T MATRIX

In this appendix we give the complete expression for the $\hat{T}$ matrix corresponding to the scattering by a strip on which both the film thickness and the speed of sound are modified. Defining $\phi=2\zeta aN/c$ and $\zeta=E\pm i\epsilon$, where $\epsilon\to 0$ and the $+$ $(-)$ sign is chosen in the case of $\langle p\,|\,\hat{T}^{+}\,|\,p_1\rangle$ ($\langle p\,|\,\hat{T}^{-}\,|\,p_1\rangle$), we obtain

$$\begin{aligned}\langle p\,|\,\hat{T}^{\pm}\,|\,p_1\rangle=&p_1^2c^2(N^2-1)(\zeta^2-c^2p^2)[\pi D_\zeta(p_1)(p_1-p)]^{-1}\sin[(p_1-p)a]\\&+2p_1c^2[\pi D_\zeta(p)D_\zeta(p_1)]^{-1}[(rN-1)^2\exp(\pm i\phi)-(rN+1)^2\exp(\mp i\phi)]\\&\times(N[A_\zeta(p)B_\zeta(p_1)+pp_1r\zeta^2c^2(N^2-1)^2]\sin[(p_1+p)a]\pm i\zeta cN(N^2-1)[p_1A_\zeta(p)+rpB_\zeta(p_1)]\cos[(p_1+p)a]\\&+\{(Nr\cos\phi\mp i\sin\phi)[B_\zeta(p_1)D_\zeta(p)+pp_1c^2(N^2-1)(\zeta^2-c^2p^2)]\\&+(\cos\phi\mp iNr\sin\phi)N[(\zeta^2-c^2p^2)B_\zeta(p_1)+pp_1c^2r(N^2-1)D_\zeta(p)]\}\\&\times\sin[(p_1-p)a]+(N^2-1)\zeta c\{(-\sin\phi\mp irN\cos\phi)pB_\zeta(p_1)\\&+Np_1(Nr\sin\phi\pm i\cos\phi)[\zeta^2-c^2p^2-rD_\zeta(p)]\}\cos[(p_1-p)a])\,.\end{aligned}\tag{A1}$$

Here we have used the following auxiliary functions:

$$A_\zeta(p)=\zeta^2(N^2r-1)+c^2p^2(1-r)\,,\tag{A2}$$

$$B_\zeta(p)=\zeta^2N^2(1-r)+c^2(rN^2-1)p^2\,,\tag{A3}$$

and

$$D_\zeta(p)=\zeta^2N^2-p^2c^2\,.\tag{A4}$$

The following special values, for $p=E/c$, are useful:

$$\begin{aligned}\langle p\,|\,\hat{T}^{+}\,|\,p\rangle=&\left[\frac{Ec}{\pi}\right]\left[\frac{2rN\cos(2EaN/c)+i(N^2r^2+1)\sin(2EaN/c)}{4r^2N^2+(N^2r^2-1)^2\sin^2(2EaN/c)}\right]\\&\times[2irN\cos(2EaN/c)+(N^2r^2+1)\sin(2EaN/c)-2irN\exp(-2iEa/c)]\end{aligned}\tag{A5}$$

and

$$\langle p\,|\,\hat{T}^{+}\,|\,-p\rangle=\left[\frac{Ec}{\pi}\right]\left[\frac{2rN\cos(2EaN/c)+i(N^2r^2+1)\sin(2EaN/c)}{4r^2N^2+(N^2r^2-1)^2\sin^2(2EaN/c)}\right](N^2r^2-1)\sin(2EaN/c)\exp(-2iEa/c)\,.\tag{A6}$$

The ratio F/A between the transmitted and the incident amplitudes for a single scatterer is

$$\frac{F}{A}=\frac{4rN\exp(-2iEa/c)}{(rN+1)^2\exp(-4iEaN/c)-(rN-1)^2}\ . \tag{A7}$$

This immediately yields the transmission coefficient.

APPENDIX B: THE EFFECTS OF INTRINSIC DISSIPATION

Although there are not many experimental data on Γ, it is reasonable to assume it is a function of the substrate.[31] Indeed, it is quite possible that it is considerable higher for a film on a rough substrate. A complete theory should introduce two Γ's, one accounting for dissipation on the original substrate, and the other accounting for dissipation on the strips. However, since intrinsic dissipation effects at low temperatures are expected to be small, it seems sensible to take a single effective damping constant valid everywhere. For simplicity, we also consider only vDW scatterers ($c_s=c$). It is easy to extend the analysis to the $c_s\neq c$ case, but the formulas become far more cumbersome. The formalism is the same as in Sec. II B, except that Eq. (2.11) must be modified to read

$$\langle x\,|\,\hat{G}^{\pm}_{E,0}\,|\,x'\rangle=-\left[(E\pm i\epsilon)^2+c^2\frac{\partial^2}{\partial x^2}+i(E\pm i\epsilon)\Gamma\right]^{-1}\delta(x-x')\ , \tag{B1}$$

with the consequent modification in Eq. (2.17).

The T-matrix elements are

$$\langle p\,|\,\hat{T}^{\pm}(E)\,|\,p_1\rangle=\frac{2c^2p_1(r-1)}{\pi}\left[\frac{(r-1)\sin[(p+p_1)a]+(r+1)\exp(\mp 2i\alpha^{\pm}a)\sin[(p_1-p)a]}{(r+1)^2\exp(\mp 2i\alpha^{\pm}a)-(r-1)^2\exp(\pm 2i\alpha^{\pm}a)}\right], \tag{B2}$$

where $\alpha^{\pm}=[(E\pm i\epsilon)/c][1+i\Gamma/(E\pm i\epsilon)]^{1/2}$. Although the symmetry relations (2.19b) and (2.19c) are still valid, it is clear that $\langle p\,|\,\hat{T}^{+}\,|\,p_1\rangle$ and $\langle p\,|\,\hat{T}^{-}\,|\,p_1\rangle$ are not the complex conjugates of each other. The optical theorem is also slightly modified due to dissipation inside of the scatterer: Writing $\alpha^{\pm}\simeq E/c+i\Gamma/2c$, which is an extremely good approximation, since $\Gamma\ll E$ for almost all E, we obtain

$$\begin{aligned}\mathrm{Im}\langle p\,|\,\hat{T}^{\pm}\,|\,p\rangle=&\pm(\pi/4Ec)(1+r^2)^{-1}[(1+r)^2\exp(\pm\Gamma a/c)+(1-r)^2\exp(\mp\Gamma a/c)]\\&\times(\langle p\,|\,\hat{T}^{+}\,|\,p\rangle\langle p\,|\,\hat{T}^{-}\,|\,p\rangle+\langle p\,|\,\hat{T}^{+}\,|\,-p\rangle\langle -p\,|\,\hat{T}^{-}\,|\,p\rangle)\ ,\end{aligned} \tag{B3}$$

for $p=E/c$. If $\Gamma=0$, we recover the usual expression for particle-number conservation.

The equation for $G^{+}_{E}(x,x')$ can be easily obtained:

$$G^{+}_{E}(x,x')=(1/2\pi)\int_{-\infty}^{\infty}dp\frac{e^{ip(x-x')}}{c^2p^2-E^2-i\Gamma E-R(E,r)np\sin(2pa)}\ , \tag{B4}$$

with

$$R(E,r)=4c^2(r-1)^2\left[\frac{H_-\cos\eta+iH_+\sin\eta}{H_-^2+4(1-r^2)^2\sin^2\eta}\right]. \tag{B5}$$

Here, $\eta=2Ea/c$, and

$$H_{\pm}=(1+r)^2\exp(\Gamma a/c)\pm(1-r)^2\exp(-\Gamma a/c)\ . \tag{B6}$$

The renormalized speed of sound and the effective attenuation can be found with the aid of the approximation used to evaluate the integral in (2.24). We obtain

$$\tilde{c}=c\left[1-\frac{na(r-1)^2H_-\sin(2\eta)}{2\eta[4r^2+(r^2-1)^2\sin\eta]}\right] \tag{B7}$$

and

$$\tilde{\Gamma}=\Gamma+\frac{4cnH_+(r-1)^2\sin^2\eta}{(H_-)^2+4(r^2-1)^2\sin^2\eta}\ . \tag{B8}$$

For small values of Γ, these formulas are simplified if we approximate $H_+\to 2(1+r^2)$ and $H_-\to 4r$.

It is worth pointing out that the introduction of a finite Γ leads to a modification of the kinetic equation (3.10), in which the term $2i\Gamma E$ should be added inside the square brackets on the left-hand side.

[1]N. F. Mott and W. D. Twose, Adv. Phys. **10**, 107 (1961).
[2]R. E. Borland, Proc. Soc. London, Ser. A **274**, 529 (1963).
[3]K. Ishii, Suppl. Prog. Theor. Phys. **53**, 77 (1973).
[4]A. A. Gogolin, Phys. Rep. **86**, 1 (1982).
[5]P. Erdös and R. C. Herndon, Adv. Phys. **31**, 65 (1982).
[6]I. Ya Gol'dshtein, S. A. Molchanov, and L. A. Pastur, Funct. Anal. Appl. **11**, 1 (1977).
[7]H. Kunz and B. Souillard, Commun. Math. Phys. **78**, 201 (1980).
[8]R. Carmona, Duke Math. J. **49**, 191 (1982).
[9]N. F. Mott, J. Non-Cryst. Solids **1**, 1 (1968).
[10]N. F. Mott and E. A. Davis, *Electronic Processes in Non-Crystalline Materials,* 2nd ed. (Clarendon, Oxford, 1979).
[11]I. N. Lifschitz and V. Ya. Kirpichenkov, Zh. Eksp. Teor. Fiz. **77**, 989 (1979) [Sov. Phys.—JETP **50**, 499 (1980)].
[12]M. Ya. Azbel, Solid State Commun. **37**, 789 (1981).
[13]M. Ya. Azbel, Phys. Rev. B **28**, 4106 (1983).
[14]M. Ya. Azbel, Solid State Commun. **45**, 527 (1983).
[15]M. Ya. Azbel, and D. P. DiVincenzo, Solid State Commun. **49**, 949 (1984).
[16]B. L. Altshuler and A. G. Aronov, Zh. Eksp. Teor. Fiz. **77**, 2028 (1979) [Sov. Phys.—JETP **50**, 968 (1979)]; B. L. Altshuler, A. G. Aronov, D. E. Khmelnitskii, and A. I. Larkin, in *Quantum Theory of Solids,* edited by I. M. Lifshitz (Mir, Moscow, 1982).
[17]The recent literature is vast. See, for example, A. B. Fowler, A. Hartstein, and R. A. Webb, Phys. Rev. Lett. **48**, 196 (1982); R. F. Kwasnick, M. A. Kastner, J. Melngailis, and P. A. Lee, *ibid.* **52**, 224 (1984); P. A. Lee, *ibid.* **53**, 2042 (1984); A. D. Stone and P. D. Lee, *ibid.* **54**, 1196 (1985); J. C. Licini, G. J. Dolan, and D. J. Bishop, *ibid.* **54**, 1585 (1985); Y. Gefen and G. Schön, Phys. Rev. B **30**, 7323 (1985); A. D. Stone, M. Ya. Azbel, and P. A. Lee, *ibid.* **31**, 1707 (1985); J. T. Masden, and N. Giordano, *ibid.* **31**, 6395 (1985); S. J. Bending and M. R. Beasley, Phys. Rev. Lett. **55**, 324 (1985).
[18]P. W. Anderson, in *Localization, Interaction, and Transport Phenomena,* edited by B. Kramer, G. Bergmann, and Y. Bruynseraede (Springer-Verlag, Berlin, 1985).
[19]J. Jäckle, Solid State Commun. **39**, 1261 (1981).
[20]A. R. McGurn, A. A. Maradudin, and Vittorio Celli, Phys. Rev. B **31**, 4866 (1985).
[21]V. Baluni and J. Willemsen, Phys. Rev. B **31**, 3358 (1985).
[22]J. B. Pendry and P. D. Kirkman, J. Phys. C **17**, 6711 (1984).
[23]C. A. Condat and T. R. Kirkpatrick, Phys. Rev. B **32**, 495 (1985).
[24]S. John, H. Sompolinsky, and M. J. Stephen, Phys. Rev. B **27**, 5592 (1983).
[25]S. Cohen and J. Machta, Phys. Rev. Lett. **54**, 2242 (1985).
[26]See, for example, H. Ishimaru, *Wave Propagation and Scattering in Random Media* (Academic, New York, 1978), Vols. 1 and 2; P. M. Morse and K. Ingard, *Theoretical Acoustics* (McGraw-Hill, New York, 1968), Chap. 8; H. Goldberger and K. Watson, *Collision Theory* (Wiley, New York, 1964), Chap. 11.
[27]T. R. Kirkpatrick, Phys. Rev. B **31**, 5746 (1985).
[28]D. Vollhardt and P. Wölfle, Phys. Rev. B **22**, 4666 (1980); P. Wölfle and D. Vollhardt, in *Anderson Localization,* edited by Y. Nagaoka and M. Fukuyama (Springer-Verlag, Berlin, 1982).
[29]See, for example, K. R. Atkins and I. Rudnick, in *Progress in Low Temperature Physics,* edited by C. T. Gorter (North-Holland, Amsterdam, 1970), Vol. 6.
[30]M. W. Cole and E. Vittoratos, J. Low Temp. Phys. **22**, 223 (1976).
[31]J. E. Rutledge and J. M. Mochel, Phys. Rev. B **30**, 2569 (1984).
[32]R. A. Guyer, Phys. Rev. B **31**, 2713 (1985).
[33]C. A. Condat and T. R. Kirkpatrick, Phys. Rev. B **32**, 4392 (1985).
[34]D. T. Smith and R. B. Hallock (unpublished).
[35]T. R. Kirkpatrick and J. R. Dorfman, in *Fundamental Properties in Statistical Physics,* edited by E. G. D. Cohen (North-Holland, Amsterdam, 1985), Vol. VI.
[36]D. J. Thouless, Phys. Rep. **13c**, 94 (1974).
[37]A. J. McKane and M. Stone, Ann. Phys. **131**, 36 (1981).
[38]D. J. Thouless, J. Phys. C **6**, L49 (1973).
[39]M. S. Lu, M. Nelkin, and M. Arita, Phys. Rev. B **10**, 2315 (1974).